ARMY RESEARCH LABORATORY

GHz Modulators in the Mid-Infrared Using Ultra High Confinement Waveguides

Lawrence C. West, Charles W. Roberts, Emil C. Piscani,
Madan Dubey, Kenneth A. Jones and George F. McLane

ARL-TR-942 August 1996

DISCLAIMER NOTICE

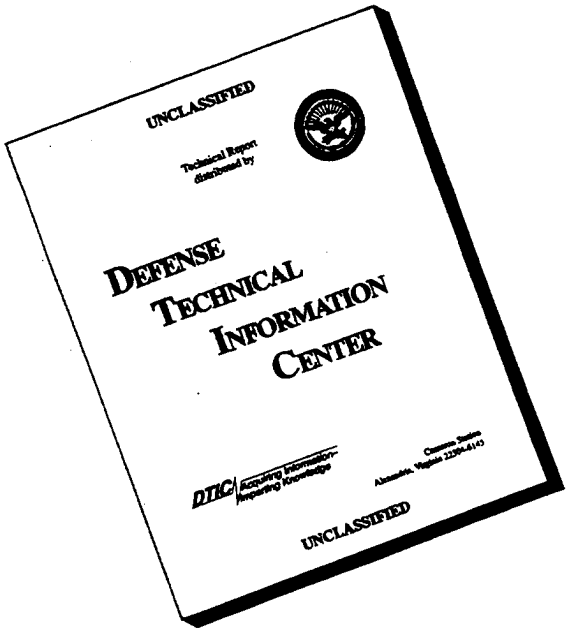

THIS DOCUMENT IS BEST QUALITY AVAILABLE. THE COPY FURNISHED TO DTIC CONTAINED A SIGNIFICANT NUMBER OF PAGES WHICH DO NOT REPRODUCE LEGIBLY.

NOTICES

Disclaimers

The findings in this report are not to be construed as an official Department of the Army position, unless so designated by other authorized documents.

The citation of trade names and names of manufacturers in this report is not to be construed as official Government endorsement or approval of commercial products or services referenced herein.

REPORT DOCUMENTATION PAGE

Form Approved
OMB NO. 0704-0188

1. AGENCY USE ONLY *(Leave blank)*	2. REPORT DATE	3. REPORT TYPE AND DATES COVERED
	August 1996	Technical Report

4. TITLE AND SUBTITLE
GHz MODULATORS IN THE MID-INFRARED USING ULTRA HIGH CONFINEMENT WAVEGUIDES

5. FUNDING NUMBERS

6. AUTHOR(S)
Lawrence C. West,* Charles W. Roberts,* Emil C. Piscani,* Madan Dubey, Kenneth A. Jones, and George F. McLane

7. PERFORMING ORGANIZATION NAMES(S) AND ADDRESS(ES)
US Army Research Laboratory (ARL)
Physical Sciences Directorate
ATTN: AMSRL-PS-DB
Fort Monmouth, NJ 07703-5601

8. PERFORMING ORGANIZATION REPORT NUMBER
ARL-TR-942

9. SPONSORING / MONITORING AGENCY NAME(S) AND ADDRESS(ES)

10. SPONSORING / MONITORING AGENCY REPORT NUMBER

11. SUPPLEMENTARY NOTES
*Lawrence West, Charles Roberts and Emil Piscani are with Integrated Photonic Systems Inc., 1325 Campus Parkway, Suite 214, Wall, NJ 07719.

12a. DISTRIBUTION / AVAILABILITY STATEMENT
Approved for public release; distribution is unlimited.

12 b. DISTRIBUTION CODE

13. ABSTRACT ***(Maximum 200 words)***

A high speed modulator at low voltage is created in the mid-infrared at 10 μm wavelengths by using field-induced absorption on otherwise forbidden intersubband transitions. The physical effects could scale to 1.5 μm wavelength light. This modulator is packaged into a unique 3.50 μm long ultra high confinement (UHC) waveguide for low capacitance and high speed. The modulator quantum wells are at the interface of a 2.1 μm thick by 3.75 μm wide UHC Ge waveguide and the GaAs substrate. The quantum wells have a 17% power coupling to the evanescent fields of the GE waveguide. A connector to the UHC waveguides, with dimensions much smaller than a free space wavelength, has been developed and demonstrated using diffractive optical element arrays on the back side of the substrate and non-uniform grating couplers. Fields are applied across the modulator quantum wells via an ohmic contact to the side of the Ge waveguide on the top of the QWs. The ground is on the other side of the waveguide and lower towards the substrate. The 7 μm wide mesa supporting the quantum wells on the bottom of the Ge waveguide is slightly wider to accommodate a gold electrode.

14. SUBJECT TERMS
Ultra High Confinement Waveguides; UHC; diffractive optical elements; grating couplers; mid-infrared; modulators; integrated optics; Ge epitaxy

15. NUMBER IF PAGES
16

16. PRICE CODE

17. SECURITY CLASSIFICATION OR REPORT	18. SECURITY CLASSIFICATION OF THIS PAGE	19. SECURITY CLASSIFICATION OF ABSTRACT	20. LIMITATION OF ABSTRACT
Unclassified	Unclassified	Unclassified	UL

CONTENTS

FIGURES

TABLE

GHz Modulators in the Mid-Infrared Using Ultra High Confinement Waveguides

1. ABSTRACT

A high speed modulator at low voltage is created in the mid-infrared at 10 μm wavelengths by using field-induced absorption on otherwise forbidden intersubband transitions. The physical effects could scale to 1.5 μm wavelength light. This modulator is packaged into a unique 350 μm long ultra high confinement (UHC) waveguide for low capacitance and high speed. The modulator quantum wells are at the interface of a 2.1 μm thick by 3.75 μm wide UHC Ge waveguide and the GaAs substrate. The quantum wells have a 17% power coupling to the evanescent fields of the Ge waveguide. A connector to the UHC waveguides, with dimensions much smaller than a free space wavelength, has been developed and demonstrated using diffractive optical element arrays on the back side of the substrate and non-uniform grating couplers. Fields are applied across the modulator quantum wells via an ohmic contact to the side of the Ge waveguide on the top of the QWs. The ground is on the other side of the waveguide and lower towards the substrate. The 7 μm wide mesa supporting the quantum wells on the bottom of the Ge waveguide is slightly wider to accommodate a gold electrode.

2. OVERVIEW

2.1 Background.

The observation of large-dipole infrared intersubband transitions in semiconductor quantum wells[1] has stimulated significant interest in semiconductor heterostructure infrared detectors, modulators, and emitters.[2] The intersubband transition has a very strong oscillator strength,[1] ideal for a high contrast modulator. This paper discusses our progress on creation of high speed (>GHz) modulation of mid-infrared light in large arrays using the intersubband transition. The applications for such arrays include spatial light modulators for parallel electric to optical interfaces for optical computing systems,[3] dynamic infrared scene projection for infrared system diagnostics, and single sideband focal plane modulator arrays for lidar and molecular sensing of mid-infrared.

The Stark shift in the energy of the transition between the first and second conduction quantum well subbands, hereafter denoted as the 1-2 intersubband transition, in a GaAs quantum well was used to create a modulator.[5] Infrared absorption modulation of the 1-2 intersubband transition was an observed result of carrier depletion in a Schottky barrier structure.[6] The modulator proposed here uses a different principle than Stark shifts or carrier depletion. The reason is our objective of low voltage modulation at high speeds with good contrast. The use of a Stark shift[5] requires a field sufficiently large to shift the intersubband resonance by a large fraction of the linewidth for high contrast modulation. Even with relatively large electric fields (>10^5 V/cm) these modulators have low (<5:1) contrast. The second approach to modulation with the intersubband transition uses carrier depletion in a Schottky barrier structure.[6] This device is capable of fair contrast with lower fields but is limited in response time by the carrier transport through the wells, and the contrast is limited by incomplete carrier depletion.

2.2 Inducing forbidden transitions for modulation.

We have proposed and demonstrated yet a new type of modulator based on 1-3 intersubband transition,[7] which is normally forbidden in a symmetric quantum well. By applying a field across the well, we break the symmetry and induce a dipole between the first and third states that increases linearly with field. The absorption is thereby created proportional to the square of the internal electric field. In this approach, the intersubband absorption is created, rather than Stark shifted, by the applied fields and starts at a zero value. Thus arbitrarily low voltages may be used while maintaining high contrast using long absorption path lengths. Also, the effect is caused by electric field effects on the quantum mechanics of the individual well potential and wavefunctions, and does not require charge transport between wells, allowing higher speeds limited primarily by the electronic interfacing.

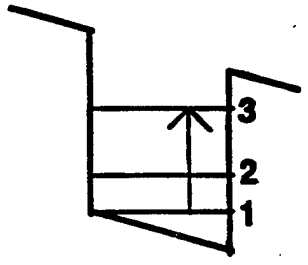

Figure 1. *The forbidden intersubband transition used for modulation.*

GaAs is naturally a low loss material in the mid-infrared region. Remaining free electron absorption may limit the practical lower value for absorption rate, but this background level can be minimized with careful choice of device doping, geometry, and pinning of the electrons in quantum wells. However, increased path lengths increase capacitance of the electrodes. creating limits to bandwidth in some electrical circuits. Fortunately, practical lengths appear small enough, under 100 micrometers, to provide sub-picofrarad capacitance for electrical interfaces into the 10's of GHz range.

2.3 The physics of a quantum well modulator.

The direction of quantization in the well is taken here to be in the z direction. The dipoles between allowed QWEST transitions are then in the z direction.[1] We initially assume a symmetric quantum well potential about z=0 with no field applied. The dipole, z_{nm}, between two envelope wavefunctions, ψ_n and ψ_m, is typically defined as

$$z_{nm} \equiv <\Psi_n|z|\Psi_m> \equiv \int \Psi_n z \Psi_m \, dz. \tag{1}$$

In quantum wells the normal electric field may not be uniform and, in particular, jump at dielectric boundary of the quantum well and its barrier. For GaAs wells and A1As barriers, the DC dielectric constants are 12.85 and 10.9 respectively, so the electric field will increase by 18 percent in the barrier region. For absorption, better accuracy can be obtained by using a definition for the dipole that is weighted by the normal electric field, which is inversely proportional to the dielectric constant. We define a new weighted dipole, $z_{nm}^{\varepsilon(\omega)}$, by

$$z_{nm}^{\varepsilon(\omega)} \equiv \int \Psi_n(z) z \frac{\varepsilon_W(\omega)}{\varepsilon(z,\omega)} \Psi_m(z) dz \tag{2}$$

where $\varepsilon_W(\omega)$ is the dielectric in the quantum well. This definition is applicable to both modulating electric fields near DC and infrared electric fields at high frequency, although this dipole will be slightly frequency dependent through the dielectric constant. We define a new weighted dipole $z_{nm}^{\varepsilon(\omega)}$, by

$$z_{nm}^{\varepsilon(\omega)} \equiv \int \Psi_n(z) z \frac{\varepsilon_W(\omega)}{\varepsilon(z,\omega)} \Psi_m(z) dz \tag{2}$$

where $\varepsilon_W(\omega)$ is the dielectric in the quantum well. This definition is applicable to both modulating electric fields near DC and infrared electric fields at high frequency, although this dipole will be slightly frequency dependent through the dielectric constant. We define the dipole for the DC and infrared frequencies by

$$z_{nm}^{DC} = z_{nm}^{\varepsilon(0)} \text{ and } z_{nm}^{DC} = z_{nm}^{\varepsilon(\omega)} \text{ for } \omega \text{ at infrared frequencies.}$$

The dipole between the first and third states z_{13}, is known to be zero in this symmetric well.[1] The modulating electric field is now applied normal to the quantum well stack, which is also in the z direction. The induced dipole between the first and third states can now be found perturbation theory. The applied electric field, F, defines a perturbing potential H′, given by

$$H' = eF(z)z, \tag{3}$$

where e is the free electron charge. First order perturbation theory is then used to define the new wavefunctions, Ψ_n', of the new potential as

$$\Psi_n' \approx \Psi_n + \sum_{m \neq n} \frac{|\Psi_m><\Psi_m|H'|\Psi_n>}{E_n - E_m}. \tag{4}$$

Using this expression for the wavefunction, the 1-3 intersubband dipole is now given to first order by

$$<\Psi'_1|z|\Psi'_3>^{AC} \approx \sum_{j\neq 1} \frac{<\Psi_1|H'|\Psi_j><\Psi_j|z|\Psi_3>^{AC}}{E_1 - E_j} + \sum_{j\neq 3} \frac{<\Psi_1|z|\Psi_j>^{AC}<\Psi_j|H'|\Psi_3>}{E_3 - E_j} \qquad (5)$$

where it was assumed that the unperturbed dipole was zero. With our perturbation potential, given by equation (3), all terms in the numerator are dipoles, z^{ε}_{nm}, and the term eF can come out in front. For a symmetric quantum well, second order perturbation calculations add wavefunctions of the same symmetry as the original wavefunction. Thus if the original wavefunctions have zero dipole between them by symmetry considerations, then so will the original wavefunction and the second order perturbation wavefunction. Thus all perturbations to second order in H′ or F go to zero and the above equation is accurate to third order. The formula for dipoles z^{ε}_{nm}, in an infinite well is proportional[1] to $mn/(m^2-n^2)$.[2] The majority of the dipole contribution can be seen to come from coupling through the second energy level. If they exist in a finite well, the fourth level adds a few percent and the sixth level coupling adds much less than 1 percent. We find a similar ratio in finite wells, although the ratio could change significantly in unusual potentials. An approximation with an accuracy better than 1 percent is obtained with summing restricted to the second and fourth levels. The above equation reduces to

$$z'^{AC}_{13} \approx eF\left[\frac{Z^{AC}_{12}Z^{AC}_{23}}{E_1 - E_2} + \frac{Z^{AC}_{14}Z^{DC}_{43}}{E_1 - E_4} + \frac{Z^{DC}_{12}Z^{AC}_{23}}{E_3 - E_2} + \frac{Z^{DC}_{14}Z^{AC}_{43}}{E_3 - E_4}\right] \qquad (6)$$

Note this perturbation theory derivation is also valid for asymmetric wells if the unperturbed state is taken as that with Z_{13} equal to zero, although the second order terms will no longer necessarily cancel. The above parameters for dipoles and transition energies can be measured in a spectrometer from line strength and line position, respectively, using the optical formulas below. Interestingly, if the second energy level is precisely in the middle between the first and third energy levels, then to the extent the AC and DC dipoles are similar, the dipole Z'_{13} will be zero for an applied field, not allowing modulation. Unfortunately, for minimum interference from spectral tails of the stronger resonant absorption from the allowed 1-2 and 2-3 intersubband transitions, this midpoint is the best location for the second energy level.

2.4 Optical properties of a two dimensional absorber.

The absorption cross section can be found in terms of fundamental parameters for a Lorentzian lineshape with dephasing time T_2 to be[1]

$$\sigma^{mn}_P \equiv \frac{e^2 T_2 \omega}{\varepsilon_0 cnh} Z^2_{mn} \frac{1}{1+(\omega-\omega_{mn})^2 T_2^2}$$

where e is the electron charge, c is the speed of light, n is the refractive index, ε_0 is the free space dielectric constant, $\omega-\omega_{mn}$ is the difference of the laser frequency from the intersubband resonance. For an infrared plane wave traveling in a direction along the plane of symmetry of a stack of quantum wells, the absorption attenuation is given by

$$\alpha = \sigma^{mn}_P (N_{s2} - N_{s1})/d$$

where N_{S1} and N_{S2} are the two dimensional surface densities of the electrons in the quantum wells for the two quantum states. The electric field polarization is in the growth direction of the stack of quantum wells with a spacing between wells of d.

For an infrared beam incident at an internal angle, θ_1 , to the normal of a stack of quantum wells, the concept of an attenuation per unit length is no longer valid. Instead the fraction of the light incident on one side of the stack of

planar absorbers that does not appear on the other side is evaluated as the absorption fraction, AF. The net attenuation is now not dependent on quantum well spacing but only on the number of wells, W. The absorption fraction, AF, given by

$$AF_{mn} = \sigma_P^{mn}\left(N_{sm} - N_{sn}\right)W\frac{\sin 2\theta_1}{\cos\theta_1}$$

where the $\sin^2\theta_i$ in the numerator adjusts for the polarization of the TM beam not being aligned with the intersubband dipole. The $\cos\theta_i$ factor in the denominator adjust for the projected area of the beam of the well, or equivalently, the increased propagation distance away from normal incidence. The infrared beam with the TE polarization does not have intersubband absorption.

3. QUANTUM WELL DESIGN

3.1 AlGaAs Quantum Wells.

Modulators are created for infrared testing at 10 μm wavelengths. This wavelength is useful for testing the CO_2 lasers and is a convenient wavelength for AlGaAs quantum wells. Using AlGaAs, the resonant wavelength of the modulator could likely be designed anywhere in the wavelength range of 3 to 30 μm. Using InAlGaAs, the wavelength range of the modulator could possibly be extended to wavelengths as short as 1.5 μm.

Any quantum well grown must be tested to ensure the presence of the intersubband transitions, their line strength, and the energy of the transitions are correct. These parameters vary because of the doping variations and traps causing variations in the free electron concentrations of the lower state. Also, variations in well thickness and Al fraction can cause the quantum energies of the states and therefore the modulation resonances and dipoles to vary. Furthermore, the modulation dipole increases linearly with voltage, creating an absorption that increases quadratically. For the purposes of testing in the spectrometer without the need to apply electrodes to a large area, and to create a small bias to improve the voltage response of the modulator, a slight built in field is created by growth of an asymmetric modulator. The desired built-in field corresponds to an external voltage of 3 to 5 volts. This built-in field was created in the past[7] by during growth by placing the donor atoms in a delta-doping on one side of the large 180 Angstrom wide quantum well. Since the ionized electrons are mostly confined in the lower electron state near the center of the well, a built-in field of approximately 4 x 10^4 V/cm was created. More recently, this delta doping method has been found to broaden the transitions and doping in the barrier regions in preferred. The narrow transitions help to increase the modulation absorption of the 1-3 intersubband transition and greatly reduce the residual absorption from the resonance tails of the 1-2 and 2-3 intersubband transitions. The built-in field is now created by use of a small step in the center of the well with an Al fraction of 2.5%. The wavefunctions and band diagram of this new structure are shown in figure 2. The energy of the $Al_{0.4}Ga_{0.6}As$ barrier is 300 meV. An 80 Angstrom thick layer of $Al_{0.025}Ga_{0.975}As$ is placed on one side of the well and 80 Angstroms of GaAs on the other side of the well. The energy of the $Al_{0.025}Ga_{0.975}As$ barrier is only 18.7 meV. The energy of the lowest three quantum states are 23.2, 70.4, and 139.7 meV relative to the GaAs band edge. Note the 1-3 intersubband transition has an energy of 116 meV to modulate a CO_2 laser beam with an energy of 124 meV. The resonance is placed at a slightly lower energy since a small Stark shift in energy does occur, pulling the resonance of the 1-3 higher in energy as the absorption grows, allowing even greater contrast than predicted by the square of the voltage. Also note that we have created the 1-3 resonance with a particular energy. A broad band modulator could be created by growing multiple wells with a slight variation in well thickness. A square top-hat absorption could be obtained as a function of wavelength. In this case, all the modulation would be from induced absorption. Note the integrated absorption will be the same in both cases, so if a modulator for a laser line is desired, the line absorber has much greater absorption and modulation strength.

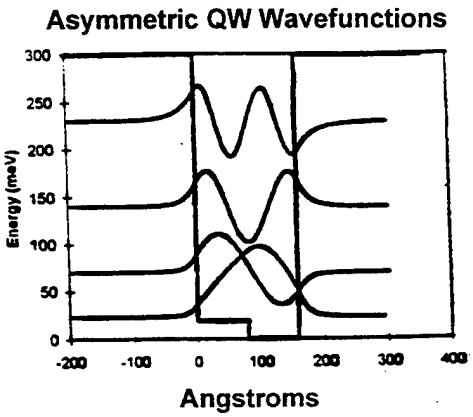

Figure 2. *The conduction band diagram and lowest four wavefunctions in the modulator QW structure.*

3.2 Electrode Physics.

A serious problem in creating a high performance modulator is that of free electron absorption. Free electrons are needed to create ohmic contact to the modulator quantum wells. This free electron absorption cross section is approximately 10^{-16} cm^2 at 10 μm wavelengths[8] and scales as the square of the wavelength. At our typical free electron levels of several times 10^{17}, this free electron absorption can be in the range of 10 to 50/cm absorption. Our modulation attenuation is in the range of 30 to 300/cm absorption so this residual free electron absorption can be equal or greater than the 1-3 intersubband absorption in the low loss modulator state, creating excessive insertion loss. For the purposes of reducing this loss, it was found that placing the electrodes in quantum wells greatly reduced this loss. The electrodes are designed so the second quantum state is barely confined by the 50 Angstrom thick $Al_{0.4}Ga_{0.6}As$ barriers to the 40 Angstrom thick GaAs wells. The intersubband resonance is broad and in the 4 μm wavelength range. Attempts were made to use electrode resonances in the far-infrared, around 25 μm wavelengths. Several problems occurred, the primary being the intersubband resonance is sufficiently strong to create a large negative index of refraction at shorter wavelengths. This lower index tends to exclude fields and lower modulation response. The total absorption of the modulator with the quantum well electrodes and the quantum well structure of figure 2 is shown in figure 3. This spectrum was taken in the spectrometer geometry of figure 4a. Note the lower lying electrodes create some residual absorption at the 10 μm wavelength of the modulator.

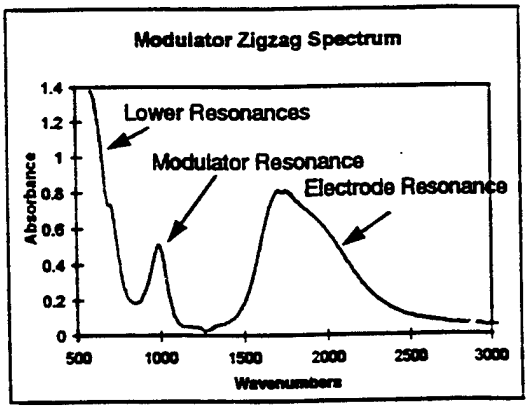

Figure 3. *Spectrum of modulator and electrode quantum wells, showing losses from electrodes.*

3.3 Modulator Performance.

The absorption was measured using an FTIR spectrometer in the zigzag geometry as shown in figure 4(a), where a six-times beam condenser was used to focus the light onto a polished end of the sample. The beam attenuation is described by the absorption fraction[1] AF given previously. In order to have a large aperture for beam coupling, the sample was polished on opposite sides at a shallow angle of $\theta_P = 17°$. The sample is L = 10mm long and d = 450 μm thick. The beam was incident on the polished surface at an angle of 45° from the z direction. In this geometry, only the TM polarization can excite the intersubband transitions (because it has a component of the field in the growth direction z).[1] In figure 4(b) it can be seen that the modulation is indeed primarily from the 1-3 intersubband absorption shown in figure 3. The modulation is mostly from induced and reduced absorption, with a small amount of energy shift observed as well. (A pure energy shift with no change in absorption line shape will show a differential absorption with equal positive and negative components.) Because the modulator quantum wells have a build-in field, the differential absorption can go negative with the removal of absorption from this built-in field.

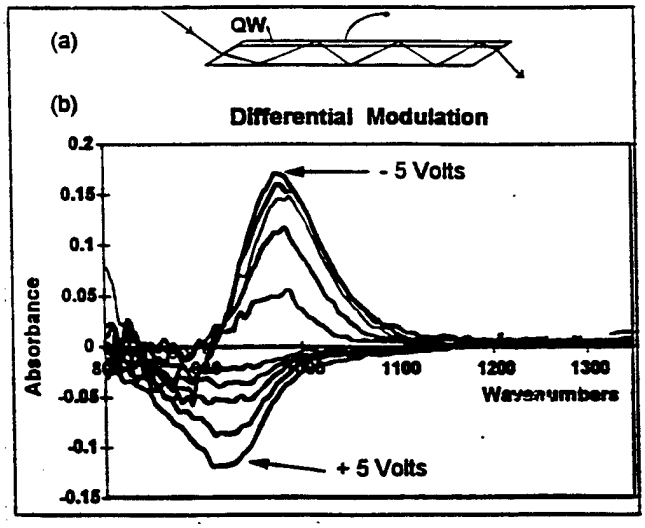

Figure 4. **(a)** *Sample geometry for differential spectrum of modulator sample.* ***(b)*** *Differential spectrum of modulator and electrodes in 1 Volt increments from -5 to 5 Volts.*

This modulator was also tested using a CO_2 laser beam at 10 μm wavelengths. A large mesa was etched on the surface of a GaAs wafer. The laser was coupled into the modulator at Brewster's angle as shown in figure 5a. The response time of this device was anticipated to be limited to 1 nsec or longer by the large area capacitance. The actual response seen here to be under 10 nsecs and was limited by the speed of our detectors. These experiments were performed at room temperature. The modulation for this single bounce through the thin quantum wells was 30% for a 20 Volt input. By use of waveguides, over 95% modulation can be obtained with only 5 Volts applied.

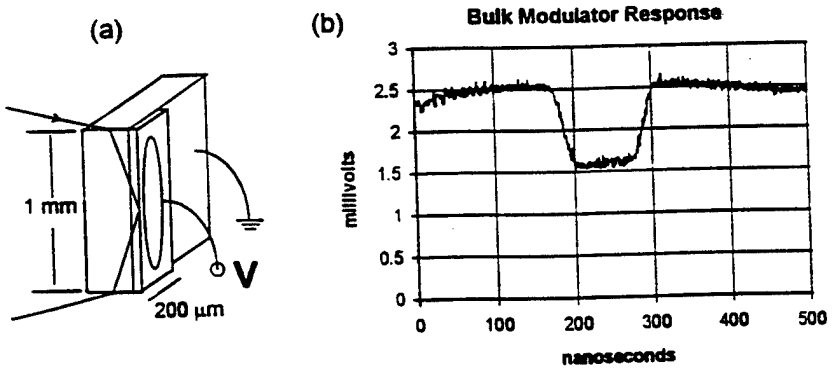

Figure 5. (a) *Coupling of laser light into modular at Brewster's angle on the cleaved edge.* (b) *The modulation response from application of a 20 Volt square wave.*

4. INTEGRATED OPTICAL DEVICES

4.1 Ge Waveguides.

The use of Ge waveguides can lower the epitaxial growth thickness from 2 μm to under 1 μm. Tight confinement of the optical beam also allows small area modulators with very low capacitance, allowing modulator speeds into the 10s of GHz. A significant problem in using Ge waveguides is the high free electron density created at the interface of Ge and the AlGaAs material from interdiffusion. This is caused by diffusion of Ge donors into GaAs, and, more seriously, by diffusion of As donors into Ge.[9] This free electron concentration creates a strong absorption that increases rapidly at the longer wavelengths. Our studies have shown that an optimal growth temperature can be found which significantly reduces the losses in the mid-infrared.[10] At low growth temperatures, a Ge oxide is formed. At high growth temperatures for the Ge, interdiffusion becomes serious as shown in figure 7. A Ge oxide is formed with low temperature growth creating a peak at 830 wavenumbers. The samples which exhibit this oxide formation have high resistance to interdiffusion upon heating to temperatures as high as 500°C, indicating at least a thin layer of this oxide material could be beneficial. The loss measurement is below the resolution of the spectrometer for the 100°C Ge growth. Therefore, slab waveguides of 2.1 μm thick Ge on GaAs have been made using the 100°C growth temperature.

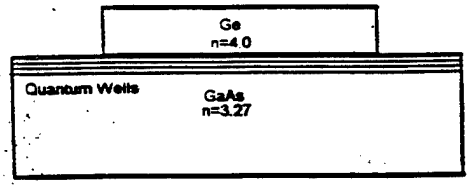

Figure 6. *A 2 μm high Ge waveguide confines 10 μm light with evanescent coupling to the active 1 μm thick QWs.*

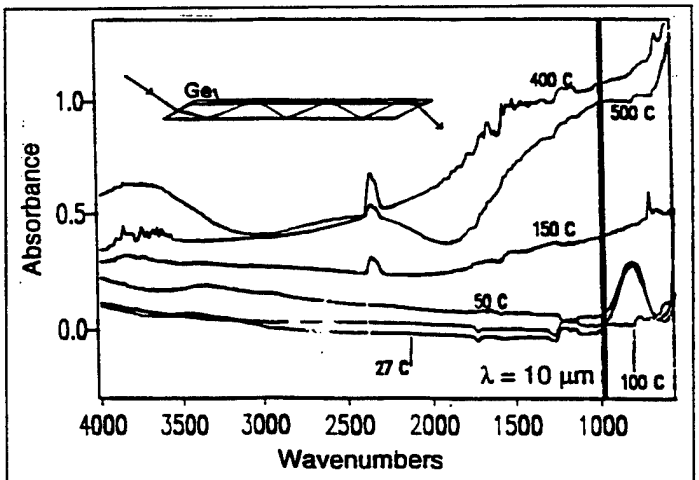

Figure 7. *Spectral absorption of 0.5-1.5 μm thick Ge films, showing an optimal growth temperature to be around 100°C. At lower temperatures, an oxide peak forms at 830 cm^{-1}. At higher growth temperatures, free electron absorption from interface diffusion becomes severe.*

Coupling to these very thin waveguides is through the use of a non-uniform grating coupler. This non-uniform coupler allows the light to scatter into

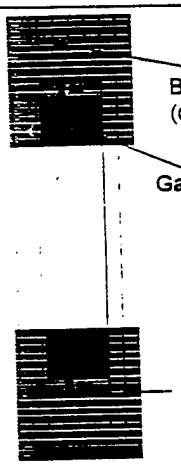

Figure 8. *The non-uniform grating coupler used to couple light into a slab Ge waveguide. Light is grating coupled at an internal angle of 21° through a beam deflector on the back side of the substrate.*

a beam profile that better matches a Gaussian for higher optical performance. The light is also scattered into the substrate at an angle of 21°, greater than the 18° total internal reflection angle. This is so the scattering is unidirectional into the substrate, reducing unwanted pathways of light scatter. By measuring the loss for a 1 mm, 2 mm, and 4 mm long waveguide, the power loss rate per length of this 100°C Ge waveguide growth has been found to be 1 l/cm. Since our induced absorption loss rate in the modulator quantum wells is in the range of 100/cm to 500/cm, this residual loss is a small effect. Our modulators need to be under 0.35 mm for high performance both electrically and optically. At this length the 1 l/cm Ge waveguide loss gives an additional 40% insertion loss. This loss should and can be improved by using proper growth techniques to limit interdiffusion.

The measured performance of the slab waveguide modulator is summarized in table I. The surface reflection is directly measured with power meters for the uncoated GaAs surface. With a proper anti-reflection coating this reflection should be reduced to 2% for a 98% efficiency. The beam deflector efficiency is measured by coupling light into a GaAs substrate without any other waveguides or couplers. At the 21° internal angle, all light is totally internally reflected into a second output beam deflector. The throughput through these deflectors is measured. Although we have created beam deflectors with greater than 90% efficiency in the past for 10 μm light using 8 levels (or three mask steps), these four-level (two mask steps) beam deflectors were expected to have a 65% efficiency. The reason for the much lower efficiency is unknown at present. The transmission through the entire structure is then measured. By removing the known efficiency of the other elements, the efficiency of the non-uniform Gaussian grating coupler can be inferred. The measured efficiency is in good agreement with our full field vector finite element time domain modeling of this grating. These non-uniform gratings have been designed for a 1.85 μm thick Ge waveguide with an efficiency approaching 90% by using several months of detailed iterations on the modeling. (Note, each model run takes 2 days on an HP 735 computer.) The recent redesign of our waveguides for a thicker 2.1 μm high Ge to allow better resonators required a total redesign of our grating coupler as well. This 55% efficiency is not yet optimized with the extensive modeling required. Our experience with more extensive numerical modeling has shown a grating efficiency of 91% should be obtainable. The measured coupler loss is now 15% transmission or an 8.2 dB coupling loss, in fair agreement with our anticipated 5.4 dB coupling loss, with the difference in numbers arising from our beam deflector. As shown in table I, this coupler efficiency is capable of being improved to over 85% transmission or less than a 0.7 dB loss per coupler.

Efficiency	Expected	Observed	Possible
Surface Reflection	0.8	0.8	0.98
Beam Deflector	0.65	0.35	0.95
Gaussian Grating	0.55	0.54	0.91
Single Couple	0.286	0.152	0.85
Double Couple	0.082	0.023	0.72

Table I. *Coupling efficiencies for various optical components involved in coupling of light to the UHC slab waveguides.*

4.2 Ultra High Confinement Waveguides and Coupler Arrays.

High speed modulators are obtained by using Ultra High Confinement (UHC) waveguides. These waveguides are 4.2 μm wide by 2.1 μm high for 10 μm wavelength light as shown in figure 9. The small size of these waveguides permits use of small area electrical contacts with small capacitance. The active QW material is placed at the interface of the Ge and GaAs where the fields are peaked. Since these waveguides are confined when the effective index is greater than the substrate index of 3.27, figure 10 shows good confinement for h greater than 0.17 times the wavelength or 1.7 μm for 10 μm light. A slightly larger size is used to minimize scattering losses in UHC resonators to be created later.

Since the dimensions of these waveguides are significantly smaller than the vacuum wavelength, external coupling through the waveguide end facets would be extremely inefficient. A method has been developed that allows large

120 μm diameter round Gaussian beams to be coupled at normal incidence to the face of the substrate through Fresnel lenses arrays on the back side of a 350 μm thick substrate (see figure 11). The external beam first illuminates an off-axis elliptical Fresnel lens which deflects the light at an angle of 21° while focusing the light to an elliptical spot with $1/e^2$ axis lengths of 120 μm long by 12 μm wide. This light is incident on a non-uniform grating coupler to a 14 μm wide by 2.1 μm high Ge waveguide. This 14 μm wide waveguide then tapers down to a 3.8 μm wide waveguide over a length of 80 μm.

The Fresnel lenses can be made to volume fill the surface of the substrate. However, it should be noted that the output lenses are on the same plane. As such the volume filling can never be better than 50% with this approach.

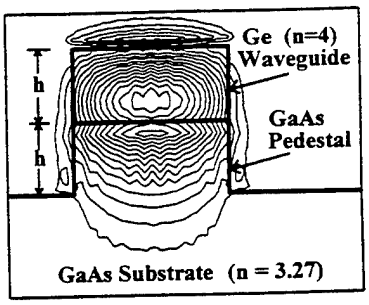

Figure 9. *Contour plot of the vertical field component in a pedestal UHC waveguide.*

Higher volume filling may be achieved by using Fresnel lenses on the front surface of the waveguide in large regions surrounding the narrow waveguides. Coupling to the front lenses would use for beam with twice the focal length to make two passes through the substrate back to the front side. A narrow reflector would be needed for the beam incident on the back side. This approach could conceivably give greater than 80% volume filling.

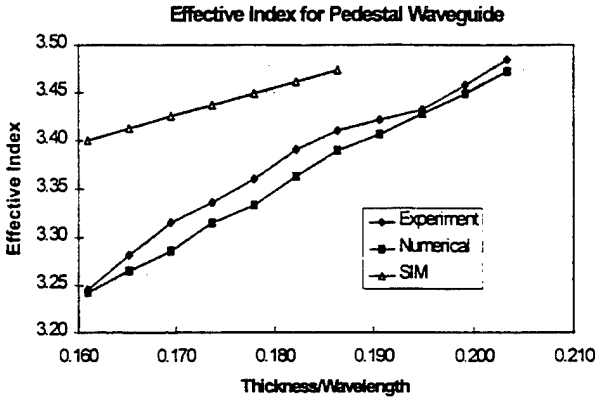

Figure 10. *The effective index of the UHC pedestal waveguide as measured by numerical modeling using time domain finite elements, a scaled experiment in the microwave, and theory using the Spectral Index Method (SIM). Note the excellent quantitative agreement between numerical modeling and experiment.*

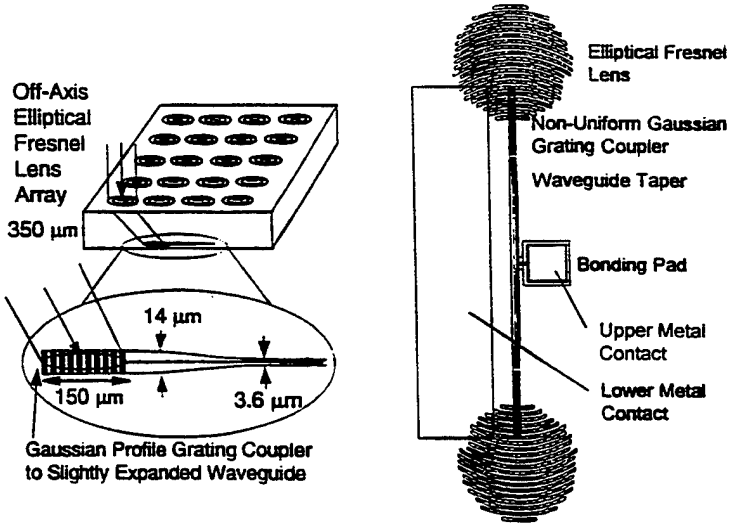

Figure 11. *Sketch of the method used to couple an array of beams into the Ultra High Confinement (UHC) waveguide modulators. The light couples through a diffractive lens on the back of the substrate to a wide waveguide with a non-uniform grating coupler and then tapers down into the narrow waveguide. Also shown is selected elements of the actual mask pattern used for this coupling and application of voltage to the modulator QWs.*

The modulator performance has not yet been measured with the UHC waveguides. From experiments with our slab waveguides and our modulation experiments, we anticipate greater than 10 to 1 contrast with 5 Volts applied. We also anticipate the 350 μm long waveguide will have a time response of approximately 5 to 10 GHz. We are presently fabricating and testing with large arrays with results from these tests expected soon.

5. SUMMARY

In summary, absorption modulators have been created in the mid-infrared using the intersubband transition. This modulator relies on the quantum induction of a 1-3 intersubband absorption. Methods have been found to modulate this transition in a device structure. A design for quantum well electrodes with low ohmic resistance and contact potential has been formed and demonstrated to significantly reduce free electron absorption, important for many mid-infrared devices. A method was found to efficiently pre-bias the modulator quantum wells with improved performance by use of an asymmetric well with 2.5% Al fraction on one side. The modulation was shown to be efficient with less than 5 volts applied. The speed of the modulation was shown to be well under 10 nsecs, as limited by capacitance and detectors used.

This modulator is being integrated into Ultra High Confinement waveguides. The coupling of Gaussian profile laser beams to the waveguide arrays is performed with diffractive optical elements (DOEs) on the back of the substrate having surface filling factors approaching unity. An off-axis elliptical lens deflects and focuses a round 120 μm diameter Gaussian beam to a 120 by 12 μm beam at an angle of 21 degrees, greater than total internal reflection. Then a periodic but non-uniform grating is used to couple the elliptical beam to a 14 μm wide waveguide of Ge on GaAs quantum wells. The efficiency of this coupling has been measured to be 15% per coupler and anticipated to improve to 85% per coupler. The waveguide is then tapered down to a 4.2 μm wide UHC waveguide. This UHC waveguide has a cross section of less than 1/20th of a square free space wavelength. Voltage is applied to the edge of the waveguide and conducted by quantum well electrodes to the Ge/GaAs interface containing the modulator layers. These device arrays are now in fabrication and expected to perform well into the gigahertz range.

6. REFERENCES

1. L. C. West and S. J. Eglash, "First observation of an extremely large-dipole transition within the conduction band of a GaAs quantum well," Appl. Phys. Lett., Vol. 46, pp. 1156-1158, June 15, 1985.

2. H. C. Liu, B. F. Levine, and J. Y. Andersson (eds.), Quantum Well Intersubband Transition Physics and Devices, Kluwer Academic Publishers, Netherlands (1994).

3. L. C. West, "Picosecond Integrated Optical Logic," Computer 20, 34 (1987).

4. R. G. Driggers, K. Barnard, E. E. Burroughs, R. G. Deep, O. Williams, "Review of infrared scene projector technology--1993," Optical Engineering, Vol. 33, pp. 2408-2417 (1994).

5. A. Harwit and J. S. Harris, Jr., Appl. Phys. Lett., Vol. 50, p. 685 (1987).

6. M. J. Kane, M. T. Emeny, N. Apsley, C. R. Whitehouse, Elect. Lett., Vol. 25, p. 230 (1989).

7. J. L. Pan, L. C. West, S. J. Walker, R. J. Malik, and J. F. Walker, "Inducing normally forbidden transitions within the conduction band of GaAs quantum wells," *Appl. Phys. Lett.*, Vol. 57, pp. 366-368, July 23, 1990.

8. J. S. Blakemore, "Semiconducting and other major properties of gallium arsenide," J. Appl. Phys., Vol. 53, pp. R123-R181, October 1982.

9. K. Sarma, R. Dalby, K. Rose, O. Aina, W. Katz and N. Lewis, J. Appl. Phys., 56, 2703 (1984).

10. M. Dubey, G. F. McLane, K. A. Jones, R. T. Lareau, D. W. Eckart, W. Y. Han, C. W. Roberts, I. P. Dunkel, L. C. West, MRS Proceeding, Vol. 340, p. 411 (1994).

Defense Technical Information Center*
ATTN: DTIC-OCC
8725 John J. Kingman Rd, STE 0944
Fort Belvoir, VA 22060-6218
(*Note: Two DTIC copies will be sent from STINFO office, Ft Monmouth, NJ)

Director
US Army Material Systems Analysis Actv
ATTN: DRXSY-MP
(1) Aberdeen Proving Ground, MD 21005

Commander, AMC
ATTN: AMCDE-SC
5001 Eisenhower Ave.
(1) Alexandria, VA 22333-0001

Director
Army Research Laboratory
ATTN: AMSRL-D (John W. Lyons)
2800 Powder Mill Road
(1) Adelphi, MD 20783-1197

Director
Army Research Laboratory
ATTN: AMSRL-DD (COL Thomas A. Dunn)
2800 Powder Mill Road
(1) Adelphi, MD 20783-1197

Director
Army Research Laboratory
2800 Powder Mill Road
Adelphi, MD 20783-1197
(1) AMSRL-OP-SD-TA (ARL Records Mgt)
(1) AMSRL-OP-SD-TL (ARL Tech Library)
(1) AMSRL-OP-SD-TP (ARL Tech Publ Br)

Directorate Executive
Army Research Laboratory
Physical Sciences Directorate
Fort Monmouth, NJ 07703-5601
(1) AMSRL-PS
(1) AMSRL-PS-A (V. Rosati)
(1) AMSRL-PS-T (M. Hayes)
(1) AMSRL-OP-FM-RM
(22) Originating Office

Advisory Group on Electron Devices
ATTN: Documents
Crystal Square 4
1745 Jefferson Davis Highway, Suite 500
(2) Arlington, VA 22202

Commander, CECOM
R&D Technical Library
Fort Monmouth, NJ 07703-5703
(1) AMSEL-IM-BM-I-L-R (Tech Library)
(3) AMSEL-IM-BM-I-L-R (STINFO Ofc)

ARMY RESEARCH LABORATORY
PHYSICAL SCIENCES DIRECTORATE
SUPPLEMENTAL DISTRIBUTION LIST
(ELECTIVE)

Deputy for Science & Technology
Office, Asst Sec Army (R&D)
(1) Washington, DC 20310

HQDA (DAMA-ARZ-D/
Dr. F.D. Verderame)
(1) Washington, DC 20310

Director
Naval Research Laboratory
ATTN: Code 2627
(1) Washington, DC 20375-5000

USAF Rome Laboratory
Technical Library, FL2810
ATTN: Documents Library
Corridor W, STE 262, RL/SUL
26 Electronics Parkway, Bldg 106
Griffiss Air Force Base
(1) NY 13441-4514

Dir, ARL Battlefield
Environment Directorate
ATTN: AMSRL-BE
White Sands Missile Range
(1) NM 88002-5501

Dir, ARL Sensors, Signatures,
Signal & Information Processing
Directorate (S3I)
ATTN: AMSRL-SS
2800 Powder Mill Road
(1) Adelphi, MD 20783-1197

Dir, CECOM Night Vision/
Electronic Sensors Directorate
ATTN: AMSEL-RD-NV-D
(1) Fort Belvoir, VA 22060-5806

Dir, CECOM Intelligence and
Electronic Warfare Directorate
ATTN: AMSEL-RD-IEW-D
Vint Hill Farms Station
(1) Warrenton, VA 22186-5100

Cdr, Marine Corps Liaison Office
ATTN: AMSEL-LN-MC
(1) Fort Monmouth, NJ 07703-5033